P2R.1 TURBULENCE STRUCTURE OF COLD SEASON CONTINENTAL STRATOCUMULUS AS OBSERVED BY THE ARM MMCR

David B. Mechem* and Yefim L. Kogan

Cooperative Institute for Mesoscale Meteorological Studies
University of Oklahoma, Norman, Oklahoma

1. INTRODUCTION

Stratocumulus clouds have a pronounced role in regulating the global shortwave radiation budget, because of their large coverage (25% of the globe; Hartman et al. 1992) and high albedo. The delicate balance between turbulent intensity, entrainment, and fluxes dictates cloud geometry and persistence, which can in turn significantly impact the radiation budget. At night, longwave flux divergence at the top of the cloud drives negatively buoyant eddies that tend to keep the boundary layer well mixed. During the day, solar absorption by the cloud is often accompanied by a reduction in turbulent intensity and a decoupling of the PBL into cloud- and sub-cloud circulations. Marine stratocumulus have been the subjects of field campaigns (e.g. Albrecht et al. 1988; 1995), numerical simulations (e.g. Moeng et al. 1986), and theoretical modeling (e.g. Lilly 1968; Stevens 2002), but relatively few studies have explored the turbulent properties of their continental cousins.

Millimeter-wavelength cloud radars (MMCRs) have been used to study the turbulent structure of boundary layer stratocumulus (e.g. Frisch et al. 1995; Kollias and Albrecht 2000). Inferring vertical velocity from the Doppler moment generally assumes that the scatterers have negligible fall speed; in other words, no precipitation is present. Thus, analysis is confined to nondrizzling or lightly drizzling cloud systems for which precipitation contamination is negligible. Under such assumptions the Doppler velocity field becomes a proxy for vertical velocity. Relative to in-situ measurements, vertical velocity from radar has the advantage of simultaneously sampling an entire column, potentially capturing the vertical coherence of the boundary layer eddy structures.

Using vertically pointing dual-wavelength (35 and 94 GHz) Doppler Millimeter-wave Cloud Radar (MMCR) and in-situ aircraft measurements, Sassen et al. (1999) showed high- and low-frequency variability (of scales 100 m and 10 km) of in-cloud vertical velocities, which they interpret to be energy from turbulent eddies and mesoscale variability, respectively. One study of Pennsylvania stratocumulus documented multiple scales, a turbulent eddy scale and a larger, topographically generated scale associated with the Allegheny Plateau (Babb and Verlinde 1999). Profiles of vertical velocity variance differ based on mean segment reflectivity, though the authors do not speculate on any physical mechanism responsible for this behavior. Kollias and Albrecht (2000) conducted an in-depth analysis of eight hours of MMCR data for a different continental stratocumulus cloud system over Pennsylvania. Vertical velocity as inferred from the MMCR Doppler velocity moment enabled the calculation of profiles of variance, skewness, cloud coverage, and mass flux.

Prior research has mainly consisted of specific case studies of cloud systems using radar scan strategies optimized for this particular cloud type. The MMCR operating at the SGP ACRF (Southern Great Plains Atmospheric Radiation Measurement Program Climate Research Facility) is broadly configured to be able to detect many different cloud types over a broad range of reflectivities and altitudes, so it is not specifically optimized for PBL clouds. Being in more-or-less continuous operation since the end of 1996, it does, however, have the advantage of long data coverage, which suggests that statistically representative measures of turbulence structure should be attainable.

This abstract summarizes the first few steps toward this goal, by classifying nonprecipitating boundary layer stratocumulus from 7 months of cold season MMCR data. Turbulence statistics from two specific cases are presented.

2. METHODOLOGY

The primary data source is the 35 GHz (K_a band) MMCR at the SGP ACRF. The radar cycles through four operating modes, each with different

*Corresponding author address: David B. Mechem, CIMMS/University of Oklahoma, 100 East Boyd, Room 1110, Norman, OK, 73019-1011

sensitivity, height coverage, and vertical resolution characteristics. The radar uses the pulse-pair method to estimate the moments of the Doppler spectrum. In each mode, data are collected over a 9 second sampling window and are then averaged. Sensitivity in some modes is boosted by coherent integration, in which the raw radar return pulses are averaged prior to signal processing. Binary phase coding, which allows for increased sensitivity at a given range resolution, is employed for some of the modes. The velocity resolution of the radar is 0.1 m s^{-1} and is an important parameter since vertical velocities in stratocumulus are typically within ±2 m s^{-1}. Details about the radar and its operational modes can be found in Moran et al. (1998) and Clothiaux et al. (1999).

We make use of the ARSCL VAP (Active Remote Sensing of Cloud Layers Value Added Product; Clothiaux et al. 2000, Clothiaux et al. 2001) to merge data from the four modes and identify cloud base and cloud top. Cloud base is estimated using data from the Belfort laser ceilometer and the micropulse lidar, and cloud top is determined from the radar data. Processing the dataset consists of classifying nonprecipitating PBL segments and performing consistency checks on cloud boundary measurements. We classify nonprecipitating PBL clouds as having:

- cloud top below 1500 m
- column maximum reflectivity of -20 dBZ

The -20 dBZ threshold conservatively identifies nondrizzling cases. However, ice phase precipitation is sometimes present at reflectivities lower than this threshold, generally when at least some part of the cloud is colder than -5 °C, the warm side of the range for the nucleation of ice phase particles. Some cloudy segments that obviously belong in the classification are excluded because of occasional radar hardware malfunctions or problems with incorrectly identified cloud boundaries (particularly cloud base). Any velocity in an echo whose reflectivity is <-35 dBZ is excluded from the analysis. While the -35 dBZ threshold is arbitrary and well within the theoretical sensitivity of the radar, Doppler velocity estimates at these low reflectivity values, particularly near cloud boundaries, are often unphysical. Enough energy may be backscattered to produce sensible reflectivities, though the velocity spectra may be seriously biased. In the future, imposing a threshold in signal-to-noise ratio, rather than reflectivity, may screen out these unrepresentative moments in a more physically meaningful way.

Once the initial data processing is complete, the vertical coordinate is transformed to a nondimensional, cloud-normalized height defined in Kollias and Albrecht (2000) as,

$$\eta = (z - z_b)/(z_t - z_b),$$

where z_b and z_t correspond to cloud base and cloud top, respectively. In the η coordinate, 0 corresponds to cloud base and 1 to cloud top. The data can then be analyzed on a segment-by-segment basis or by compositing into hour-by-hour bins in order to evaluate the diurnal cycle. In order to remove mean bias or any mesoscale variability in the velocity field, at each vertical level we subtracted from the Doppler velocity the 1 h segment mean value.

The effective data sampling frequency for boundary layer clouds lies somewhere between the sampling frequency (9 s) and the time it takes the radar to cycle through the four operational modes (~40 s). This range is generally thought to be too long to capture coherent boundary layer eddy structures, but radar scans may be thought of as tending toward independent samples, which should provide sensible statistics. In spite of conventional wisdom, a time series below shows more coherent behavior than might be expected from such a sampling strategy. One must also be aware that scans in each operational mode (~9 s) contain some form of averaging, either of the profiles themselves or coherent integration to enhance the radar sensitivity. Because of these sampling and processing details, some smoothing of the moments takes place.

3. 29 MARCH 2001 CLOUD SYSTEM

The stratocumulus cloud system occurring on 29 March 2001 occurred after the passage of a cold front at approximately 0000 UTC. The 0000-0400 UTC time period was associated with weak cold advection (surface temperature falling from 7.5 to 6 °C in four hours) and increasing pressure at the surface. Large scale subsidence most likely accompanies the increasing surface pressure and to some extent mimics the conditions over the subtropical marine stratocumulus regions. The vertical structure of the boundary layer (sounding not shown) indicates the typical thermodynamic structure of stratocumulus — a well-mixed subcloud layer and a saturated, moist adiabatic cloud region topped by an inversion. Only in the upper part of the cloud does the temperature fall below 0 °C, but the lowest temperature of ~-1.5 °C is likely not low enough for ice particle nucleation. Therefore, it is

reasonable to assume that the cloud system is composed completely of liquid water. Many of the stratocumulus systems in our cold season dataset have cloud tops as cold as -10 °C and hint of the strong possibility of ice or mixed-phase conditions. Winds backing with height are also indicative of cold advection and imply postfrontal conditions. Four hours of reflectivity and Doppler velocity data from 29 March 2001 are shown in Figure 1. Cloud top and base are remarkably stable over the period. Radar echo below cloud base hints at the presence of precipitation, particularly from 0000-0100 UTC where the vertical velocities in the lower part of the cloud and over the subcloud layer are predominantly negative. Reflectivity values are below -20 dBZ, precluding the possibility of significant liquid drizzle drops.

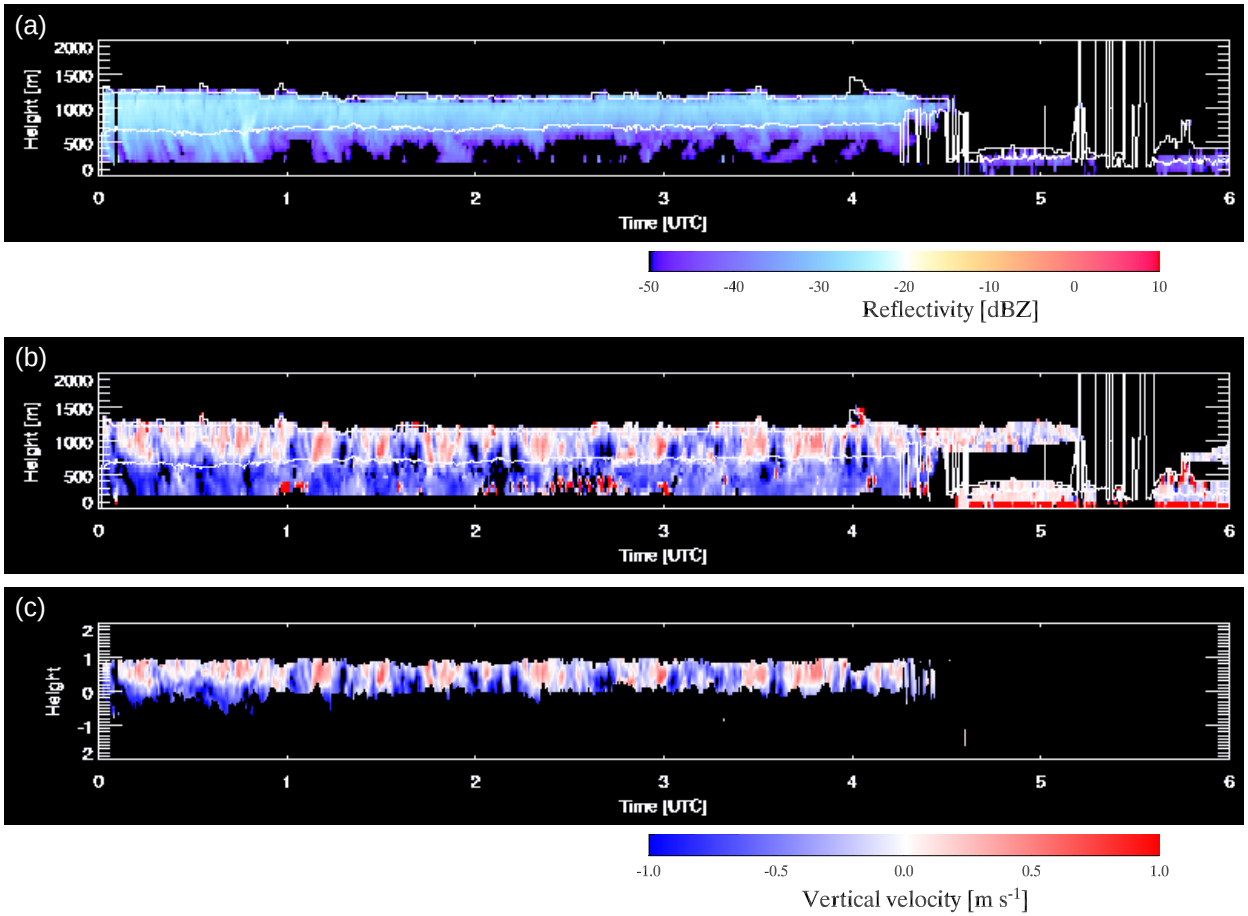

Figure 1. MMCR imagery from 0000-0600 UTC 29 March 2001. (a) Unprocessed reflectivity, plotted as a function of time and geometric height. (b) Unprocessed Doppler velocity in the geometric height coordinate. (c) Processed Doppler velocity in the transformed coordinate. A nondimensional height of 0 corresponds to the ARSCL identified cloud base; 1 corresponds to cloud top. The processing procedure is described in detail in Section 2.

The velocity time series in Figure 2 demonstrate remarkable coherence in vertical structure and time. While some of the peaks are likely smoothed by the 9 s sampling interval, the figure captures reasonably well the overall variability associated with turbulent boundary layer eddies. The updraft and downdraft maxima are weaker than in the continental case analyzed by Kollias and Albrecht (2000). We speculate that the enhanced downwelling IR from the thick cirrus deck (relative to what would be present in clear sky conditions) visible at 7-9 km AGL in the full-depth radar imagery reduces the net longwave flux and flux divergence at cloud top. This reduction in cloud top radiative forcing would result in weaker eddy structures. Postfrontal stratocumulus over the ACRF are frequently accompanied by upper level cirrus.

Mean profiles of vertical velocity variance and skewness in 3a and b, taken after sunset, show a well-mixed cloud layer but decreasing variance in the lower part of the cloud, possibly indicative of decoupled cloud and subcloud layer circulations. The magnitude of the variance is smaller than for previous continental cases (Babb and Verlinde 1999; Kollias and Albrecht 2000), which is simply a result of the smaller vertical velocities mentioned above. Skewness over the cloud layer is slightly negative, implying the predominance of strong, narrow downdrafts associated with cloud-top cooling. The skewness profile is consistent with the absence of shortwave forcing in this case.

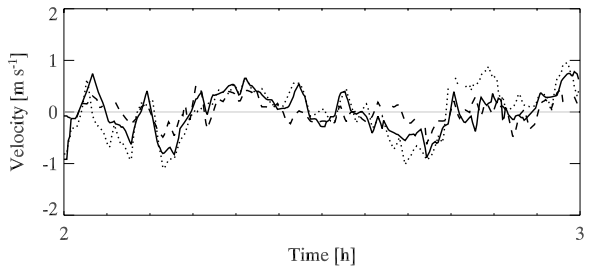

Figure 2. Time series of vertical velocity at three levels in the cloud (η = 0.25, 0.50, 0.75) from 0200-0300 UTC on 29 March 2001.

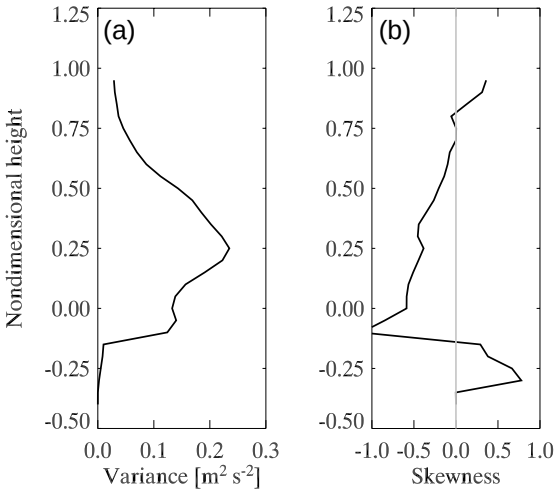

Figure 3. Vertical velocity statistics from 0200-0300 UTC 29 March 2001. (a) Variance. (b) Skewness

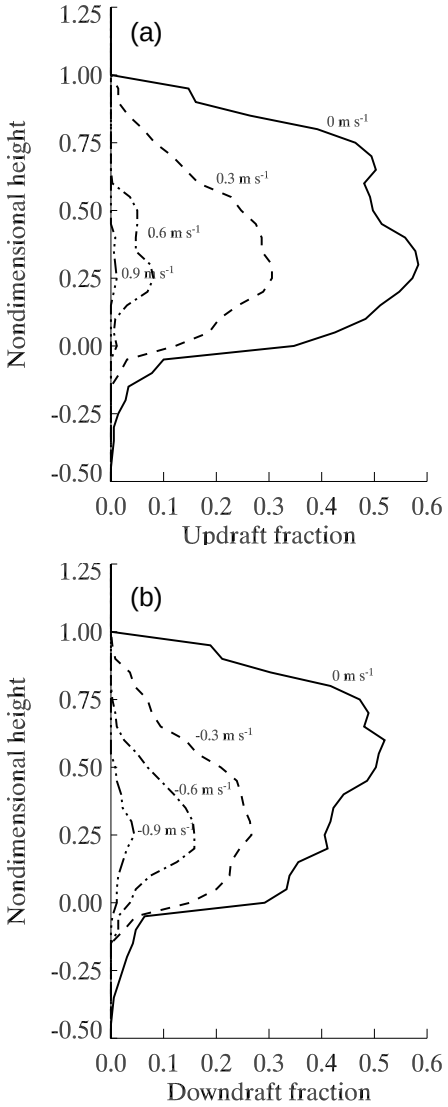

Figure 4. Vertical profiles of the fractional area of (a) updrafts and (b) downdrafts from 0200-0300 UTC. Solid lines are the fractional areas for all updrafts and downdrafts, and the dashed profiles are obtained from conditional sampling using velocity thresholds of ±0.3, ±0.6, and ±0.9 m s^{-1}.

The weakly negative skewness is also apparent in the updraft and downdraft fraction profiles in Figure 4, both of which are nearly 0.5 for all updrafts and downdrafts. The area covered by downdrafts is slightly smaller than that covered by updrafts, which is consistent with the weak negative skewness profile in Figure 3b. The total downdraft fraction is greatest near cloud top, while the updraft cloud fraction is greatest near cloud base. This result is consistent with the forcings at cloud

top and base, respectively. Downdrafts forced from cloud top cooling will be strongest near cloud top and will weaken from lateral entrainment as they move downward. Likewise updrafts forced from surface fluxes will be strongest at low levels and under entrainment will weaken with height. The ±0.6, and ±0.9 m s^{-1} conditional sample curves in Figure 4 demonstrate that strong downdrafts tend to be more common than strong updrafts. This result is also consistent with the weak negative skewness, which implies the slight predominance for narrower, stronger downdrafts and wider, weaker updrafts.

4. 3 MARCH 1997 CLOUD SYSTEM

The cloud system visible in the MMCR segment shown in Figure 5 was also associated with the passage of a cold front. The frontal passage occurred near 0800 UTC, as inferred from a surface meteogram, and was followed by decreasing temperature and increasing pressure. Thermodynamic conditions transition from a stably stratified cloud layer associated with the prior frontal precipitation into the stratocumulus boundary layer regime — a well-mixed subcloud layer, a moist adiabatic cloud layer, and an inversion. Unlike the 29 March case, which we argue is completely liquid water, in this case the cloud top reaches nearly -8 °C and likely contains ice phase particles.

Variance and skewness in Figure 6a and b calculated over two hourly periods 3 December 1997 indicate a complex behavior in turbulence. Vertical velocity variance from 1400-1500 UTC extends down into the subcloud layer, implying robust mixing in the vertical and eddies that span the entire depth of the boundary layer. By 2100-2200 UTC, the turbulent intensity is much weaker, characteristic of the suppression of turbulence several hours after peak insolation. Skewness is generally positive from 1400-1500 UTC, implying intense, narrow updrafts and a surface-based forcing. The noisy skewness profile at the later time may result from the weak vertical velocities and suppressed turbulence associated with mid-afternoon conditions.

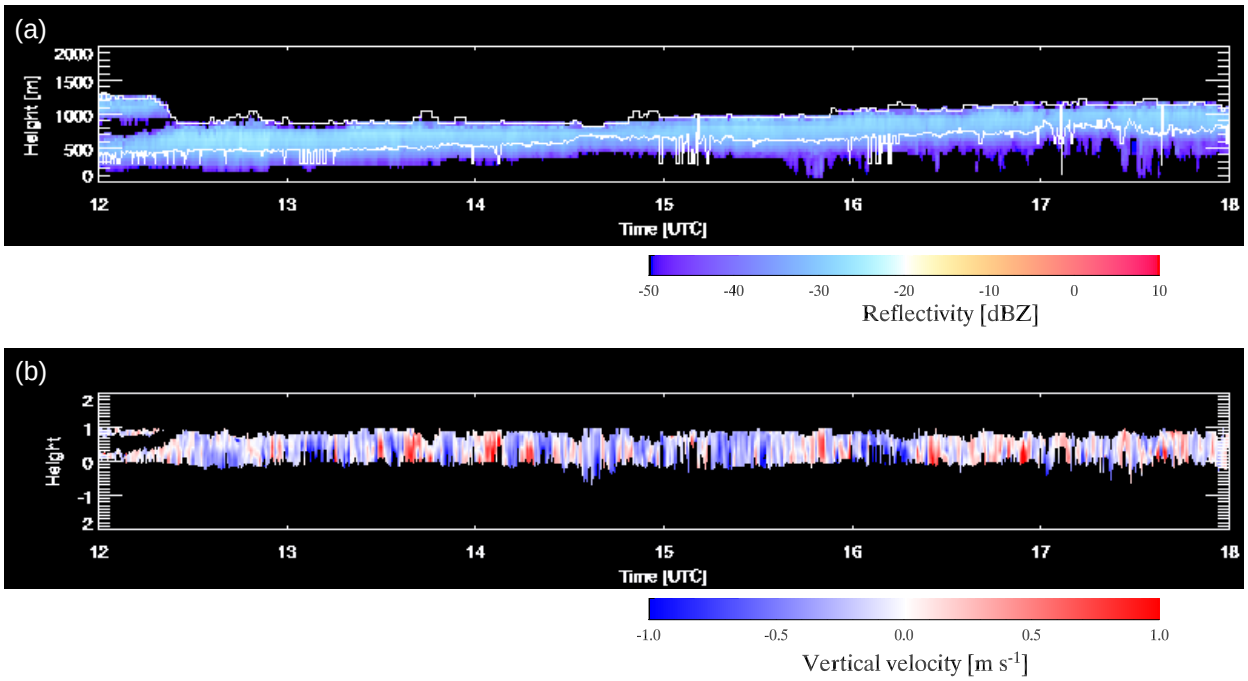

Figure 5. MMCR imagery from 1200-1800 UTC 3 December 1997. (a) Unprocessed reflectivity, plotted as a function of time and geometric height. (b) Processed Doppler velocity in the transformed coordinate η.

5. DIURNAL VARIABILITY

Profile shapes and mean turbulent intensity vary significantly over the diurnal cycle and from case-to-case. In the cases analyzed so far, turbulent intensity, represented by the vertical velocity variance, generally tends to be less than that observed in previous studies, both over marine and continental locations. This may be somewhat due to the 9 s averaging interval, or it may arise from

other effects, such as enhanced downwelling longwave flux from elevated cloud decks that frequently accompany postfrontal stratocumulus.

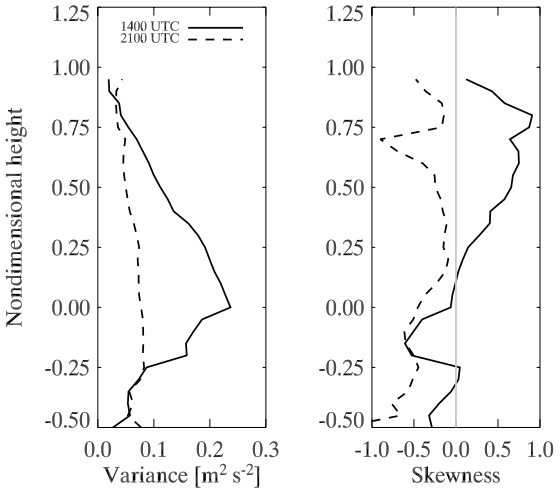

Figure 6. Variance and skewness of vertical velocity from 1400-1500 and 2100-2200 UTC 3 December 1997.

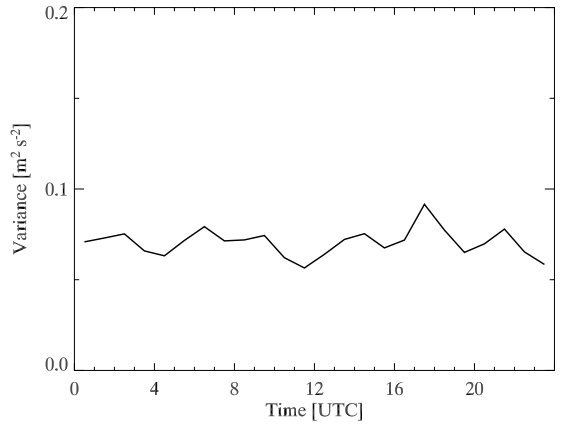

Figure 7. Diurnal cycle of cloud layer-averaged vertical velocity variance, calculated from all seven months of cold season data.

As a first attempt at identifying the presence of diurnal variability in turbulent intensity, we composited the dataset into 24 bins (for 0000-0100 UTC, 0100-0200 UTC, etc.) and calculated statistics for each bin. The data stratified in this preliminary manner show very little diurnal variability in cloud-mean velocity variance, as is evident in Figure 7. Prior results from marine stratocumulus case studies show a diurnal cycle of in-cloud turbulence strongly tied to shortwave absorption (e.g. Frisch et al. 1995). Figure 6 exhibits this behavior of different levels of cloud layer turbulence under weak and strong insolation (i.e. just after sunrise and mid-afternoon). However, because of the wide case-to-case variability in turbulence, it appears that this diurnal signal tends to be masked when averaged over all cases.

6. SUMMARY

We analyze two cases from a subset of 7 months of cold season MMCR data to demonstrate that meaningful turbulence statistics can be extracted using a 35 GHz radar and a scan strategy not optimized for sampling boundary layer turbulence. Time series show that, at least for some cases, 9 s samples are capable of capturing coherent eddy structures, both in time and in the vertical. Even when the advective speed is too great to sample coherent signals, each radar scan trends toward being an independent sample (i.e. becomes less autocorrelated); thus, meaningful statistics can still be calculated. The 9 s sampling interval for the ARM MMCR smooths the velocity data somewhat, so peak magnitudes may not be accurately represented.

Statistics of vertical velocity vary greatly from case to case. Variance tends to be a maximum over the lower part of the cloud or right at cloud base. The position of the maximum implies either a cloud layer that is decoupled from the subcloud layer or well-mixed conditions throughout the depth of the boundary layer. Skewness can be both positive or negative, which implies energetic forcing from the surface or from cloud top, respectively.

Turbulent intensity varies considerably from case-to-case and over the course of a day. We show an example of the well known behavior where solar absorption suppresses cloud layer turbulence. Although diurnal variations are visible in individual cases, compositing all 7 months of data into an ensemble of 24 hourly bins does not show a strong diurnal signal in turbulent intensity. We believe that the case-to-case variability masks the more subtle diurnal signal. It is possible that normalizing the turbulence statistics for each case might enable a meaningful comparison of case-by-case statistics.

ACKNOWLEDGEMENTS

The authors appreciate discussions with Pavlos Kollias and Eugene Clothiaux. This research was supported by the Environmental Sciences Division

of the U.S. Department of Energy (through Battelle PNR Contract 144880-A-Q1 to the Cooperative Institute for Mesoscale Meteorological Studies) as part of the Atmospheric Radiation Measurement Program, and by ONR N00014-96-1-0687 and N00014-03-1-0304.

REFERENCES

Albrecht, B. A., D. A. Randall, and S. Nicholls, 1988: Observations of marine stratocumulus clouds during FIRE. *Bull. Amer. Meteor. Soc.*, **69**, 618-626.

Albrecht, B. A., C. S. Bretherton, D. Johnson, W. H. Schubert, and A. S. Frisch, 1995: The Atlantic Stratocumulus Transition Experiment — ASTEX. *Bull. Amer. Meteor. Soc.*, **76**, 889-904.

Babb, D. M. and J. Verlinde, 1999: Vertical velocity statistics in continental stratocumulus as measured by a 94 GHz radar. *Geophys. Res. Lett.*, **26**, 1177-1180.

Clothiaux, E. E., K. P. Moran, B. E. Martner, T. P. Ackerman, G. G. Mace, T. Uttal, J. H. Mather, K. B. Widener, M. A. Miller, and D. J. Rodriguez, 1999: The Atmospheric Radiation Measurement Program cloud radars: Operational Modes. *J. Atmos. Oceanic Technol.*, **16**, 819-827.

Clothiaux, E. E., T. P. Ackerman, G. G. Mace, K. P. Moran, R. T. Marchand, M. A. Miller, and B. E. Martner, 2000: Objective determination of cloud heights and radar reflectivities using a combination of active remote sensors at the ARM CART sites. *J. Appl. Meteor.*, **39**, 645-665.

Clothiaux, E. E., M. A. Miller, R. C. Perez, D. D. Turner, K. P. Moran, B. E. Martner, T. P. Ackerman, G. G. Mace, R. T. Marchand, K. B. Widener, D. J. Rodriguez, T. Uttal, J. H. Mather, C. J. Flynn, K. L. Gaustad, and B. Ernold, 2001: The ARM millimeter wave cloud radars (MMCRs) and the active remote sensing of clouds (ARSCL) value added product (VAP), DOE Tech. Memo. ARM VAP-002.1, U. S. Department of Energy, Washington, D. C.

Frisch, A. S., D. H. Lenschow, C. W. Fairall, W. H. Schubert, and J. S. Gibson, 1995: Doppler radar measurements of turbulence in marine stratiform cloud during ASTEX. *J. Atmos. Sci.*, **52**, 2800-2808.

Hartman, D. L., M. E. Ocker-Bell, and M. L. Michelsen, 1992: The effects of cloud type on earth's energy balance: Global analysis. *J. Climate*, **5**, 1281-1304.

Kollias, P., and B. Albrecht, 2000: The turbulence structure in a continental stratocumulus cloud from millimeter-wavelength radar observations. *J. Atmos. Sci.*, **57**, 2417-2434.

Lilly, D. K., 1968: Models of cloud-topped mixed layers under a strong inversion. *Quart. J. Roy. Meteor. Soc.*, **94**, 294-309.

Moran, K. P., B. E. Martner, M. J. Post, R. A. Kropfli, D. C. Welsh, and K. B. Widener, 1998: An unattended cloud-profiling radar for use in climate research. *Bull. Amer. Meteor. Soc.*, **79**, 443-455.

Sassen, K. G. G. Mace, Z. Wang, M. R. Poellot, S. M. Sekelsky, and R. E. McIntosh, 1999: Continental stratus clouds: A case study using coordinated remote sensing and aircraft measurements. *J. Atmos. Sci.*, **56**, 2345-2358.

Stevens, B., 2002: Entrainment is stratocumulus topped mixed layers. *Quart. J. Roy. Meteor. Soc.*, **128**, 2663-2690.